




## Conversion of angular momentum into charge at picosecond timescales in the LaAlO<sub>3</sub>/SrTiO<sub>3</sub> interface

Anas El Hamdi,<sup>1</sup> Artem Levchuk <sup>1,2</sup> Cosimo Gorini <sup>1,\*</sup> Margherita Boselli,<sup>3</sup> Vincent Juvé,<sup>2</sup> Tadele Orbula Otomalo,<sup>2</sup> Gwenaëlle Vaudel <sup>2</sup> Stefano Gariglio <sup>3</sup> Pascal Ruello <sup>2</sup> Jean-Yves Chauleau,<sup>1,†</sup> and Michel Viret <sup>1</sup>

<sup>1</sup>*SPEC, CEA, CNRS, Université Paris-Saclay, 91191 Gif-sur-Yvette, France*

<sup>2</sup>*Institut des Molécules et Matériaux du Mans, UMR 6283 CNRS, Le Mans Université, 72085 Le Mans, France*

<sup>3</sup>*Département de Physique de la Matière Quantique, University of Geneva, 24 Quai Ernest-Ansermet, Genève 4, 1211, Switzerland*



(Received 15 March 2024; revised 25 June 2024; accepted 11 July 2024; published 7 August 2024)

Mechanisms of spin/charge interconversion like the spin Hall effect can be used to generate and detect spin currents at timescales ranging from dc to subpicosecond. In the dc regime, the best candidates are Rashba interfaces showing the inverse Edelstein effect, with LaAlO<sub>3</sub>/SrTiO<sub>3</sub> presenting a record conversion efficiency. At picosecond timescales, devices relying on inverse spin Hall effect are efficient THz emitters, but this is less clear for Rashba-Edelstein systems. Here we study the conversion of angular momentum into charge at different timescales in the LaAlO<sub>3</sub>/SrTiO<sub>3</sub> interface. We show that while the effect is exceptionally large in the dc regime, it is reduced by more than four orders of magnitude at the picosecond timescale. This loss of efficiency is discussed in terms of specificities linked to the Rashba state at the interface between these two large band-gap insulators. This has strong implications for the spintronic THz emitters and our work underlines the salient features required for their optimal operation.

DOI: [10.1103/PhysRevB.110.054412](https://doi.org/10.1103/PhysRevB.110.054412)

Spintronics is a research field that develops novel ways to process information and store data, using the interaction of electronic and magnetic degrees of freedom [1]. It relies on the manipulation of angular momentum, generally carried by conduction electrons experiencing spin-dependent scattering. In order to get rid of all sources of dissipation one needs to decouple charge and spin and use pure spin currents without charge motion. A central interaction between these two degrees of freedom is the spin-orbit effect, leading to spin dependent scattering of electrons in metals and semiconductors. The interaction can also interconvert spin and charge, which is essential to design spin sources or detectors to process pure spin currents. There are several spin/charge (S/C) conversion mechanisms, all based on the spin-orbit interaction. The most commonly used one is the inverse spin Hall effect [2,3] (ISHE), present in conductors with large spin-orbit coupling, such as the *5d* metals Pt or W. Recently, another mechanism based on the Rashba effect has been used for spin-to-charge conversion. It relies on the locking between linear momentum and spin of conduction electrons in a two-dimensional state subjected to a strong built-in electric field. The Rashba Hamiltonian splits an ideal parabolic band into two subbands with opposite chiral spin structures. When a charge current flows in a Rashba system a net nonzero spin accumulation occurs, emanating from the uncompensation of the Fermi contours with opposite chiralities; this is known as the Edelstein effect [4]. The reciprocal effect is called the spin galvanic or inverse Edelstein effect (IEE) [5–9], where the injection of a nonzero

spin population into a Rashba system gets converted into a charge current due to a net drift in the Fermi contours. As a consequence, these systems can act as spin-to-charge (S/C) convertors as pumping a spin population generates a transverse electrical current [10].

So far, the most efficient S/C conversion is observed in the two-dimensional electronic state (2DES) at the interface between TiO<sub>2</sub>-terminated [001] SrTiO<sub>3</sub> (STO) and another band gap insulator like LaAlO<sub>3</sub> (LAO) [7,8,11]. For thicknesses above four unit cells, a high mobility 2DES appears in the STO side because of a charge transfer mechanism preventing a diverging voltage originating from the succession of dipoles of the alternating LaO and AlO<sub>2</sub> atomic planes. Interestingly, this gives birth to Rashba spin-orbit coupling [12], which can be modulated using a back-gate voltage [13]. Indeed, the high dielectric constant of STO at low temperature and the low carrier density of the 2DES allow for an efficient gate controlled shifting of the chemical potential. This large tunability is a central characteristic of this system making it of great interest for several physical studies and potential applications. Some particular Dirac-like points of the band structure have been identified in transport measurements as a Lifshitz transition occurring when new bands of a different symmetry are populated [14,15]. In fact, this transition is best seen in measurements of the inverse Edelstein effect (IEE) where spin to charge conversion shows a clear maximum versus back-gate voltage [7,9].

The figure of merit of the IEE effect is a distance  $\lambda_{\text{IEE}}$  obtained from the ratio between the three-dimensional (3D) spin current density ( $j_s^{3D}$ ) and the resulting 2D charge current density ( $j_c^{2D}$ ).  $j_c^{2D}$  is simply the measured voltage divided by the stack resistance and the unit cell parameter

\*Contact author: [cosimo.gorini@cea.fr](mailto:cosimo.gorini@cea.fr)

†Contact author: [jean-yves.chauleau@cea.fr](mailto:jean-yves.chauleau@cea.fr)

(considering a purely 2D system). In a simple Rashba system,  $\lambda_{\text{IEE}}$  directly depends on the Rashba coupling  $\alpha_{\text{R}}$ , but also on the electron relaxation lifetime  $\tau$  through:  $\lambda_{\text{IEE}} = \frac{\alpha_{\text{R}}\tau}{\hbar}$ . Known efficient spin to charge converters have either a large Rashba splitting or a large relaxation lifetime, and no system has been found with both. Bi/Ag belongs to the first type whereas LAO/STO is in the latter category with a rather small Rashba coefficient, but a slow relaxation, conferring it an exceptional IEE [8]. Taking  $\alpha_{\text{R}} = 0.003 \text{ eV \AA}$  [16], one can estimate the lifetime to be above 10 ps, which is consistent with that extracted from magnetotransport [12] and nonlocal resistance [17,18] measurements (showing some variability). IEE lengths between 6 and 20 nm (depending on back-gate voltages) obtained for STO-based systems host the record conversion efficiency [7,8,11]. The Ag/Bi Rashba interface has  $\lambda_{\text{IEE}} \approx 0.3 \text{ nm}$  with a very short relaxation time of 5 fs but a large Rashba splitting of  $0.56 \text{ eV \AA}$  [5,6]. This can be compared to heavy metals, where  $\lambda_{\text{IEE}}$  represents the product of the spin Hall angle and the spin diffusion length, which yields values typically lower than 0.5 nm for Pt, Ta, and W [19]. Remarkably, the LAO/STO system has also been shown to very efficiently convert orbital momentum into charge [9] (the orbital equivalent to the spin IEE) and when angular momentum is injected from NiFe, slightly more than half of the charge current is coming from orbital momentum conversion. This complexifies the detailed conversion processes but does not conceptually change the problem of angular momentum conversion into charge.

Beside this quasistatic behavior, spin currents can also be handled on timescales down to a few tens of femtoseconds. Indeed, transport of spin angular momentum has been put forward as a key mechanism in light-induced ultrafast magnetization dynamics [20–22] during which bursts of angular momentum are emitted by hot electrons [23–25]. Their conversion into subpicosecond electrical transients is the source of a THz radiation [26] observed in pure ferromagnetic layers [27] or generated by magnetic and surface nonlinearities [28]. These signals can be greatly amplified by adding a spin-to-charge converter [29] and the resulting efficient THz emitters [26,29] can compete with optical rectification in ZnTe [30], GaP, and InP [31] while also providing gapless emission spectra. They represent a technological implementation of femtosecond spin currents and extensive work is devoted to improving and tailoring their emission [20]. Therefore, it is interesting to look into the options offered by IEE systems, and some work has already been published on Bi/Ag [32,33] or CoFeB/MgO [34] interfaces. However, LAO/STO, the best convertor in the dc range, has not been thoroughly studied in the ultrafast regime [35], which is the aim of the present paper.

Our measurements are performed on a five unit cell epitaxial layer of LaAlO<sub>3</sub> (LAO) deposited on top of TiO<sub>2</sub>-terminated SrTiO<sub>3</sub> by pulsed laser deposition [8]. A 12-nm-thick permalloy (NiFe) layer (passivated with 3 nm of Al) was then evaporated (in a different chamber) to provide spin injection through the LAO. The measurements are compared to those on a Co<sub>40</sub>Fe<sub>40</sub>B<sub>20</sub>(5 nm)/Pt(3 nm) bilayer, a prototypical ISHE system known to be very reliable at all timescales [26,29,34], making this system an ideal standard reference. Here, we use rf spin-pumping by ferromagnetic resonance [36] (FMR), and light-induced ultrafast

emission of hot-carrier spin currents. The S/C conversion efficiency is assessed by measuring built-in voltages across the samples using simple electrodes for quasistatic approaches and time-dependent terahertz spectroscopy for the ultrafast regime [17].

The efficiency of the LAO/STO system is first measured in the quasistatic regime, at 10 K, by radio-frequency spin-pumping experiments as shown in Fig. 1(a), where the samples are excited by a microwave magnetic field at a fixed frequency. Sweeping a dc magnetic field allows us to meet the resonance condition, corresponding to a divergence of the measured microwave absorption and leading to an exaltation of the amplitude of the magnetization precession. There, the angular momentum is absorbed and a dynamical nonequilibrium spin population is pumped into the 2D electron gas through the LAO [7,8]. We measure here the dc part of the built-in S/C voltages across the samples, shown in Fig. 1 for a rf excitation at 3.2 GHz. Experimentally the addition of a slow modulated magnetic field enables a sensitive lock-in detection so that the measured signals have the shape of a Lorentzian derivative with respect to the dc applied magnetic field. We subsequently fit these to extract all relevant parameters: amplitude, resonance field, and linewidth. The injected spin current  $j_c^{3\text{D}}$  is calculated through the FMR measurements by the difference in damping with and without the 2DES [5]. It depends on several parameters like the spin mixing conductance, the microwave power, or the magnetization of the ferromagnetic layer, which can all be extracted from the FMR study. For our samples, we find  $M_s \approx 1 \text{ T}$ , and the damping parameter  $\alpha_{\text{NiFe}/2\text{DES}} = 1 \times 10^{-2}$ . Comparing this value with our reference sample ( $\alpha_{\text{NiFe}} = 7 \times 10^{-3}$ ), one can retrieve the spin mixing conductance ( $G_{\uparrow\downarrow} \approx 10^{-19} \text{ m}^{-2}$ ) and the effective spin current density ( $j_s^{3\text{D}} = 3 \times 10^5 \text{ A m}^{-2}$ ). We would like to underline here that this procedure is questionable for IEE because spin/orbital carriers can participate in charge conversion without losing their angular momentum. Hence, the spin/orbital polarization in the 2DES is not purely determined by the *increase* of damping and it is likely that intrinsic damping itself has some relevance in the process. Nevertheless, we adopt here the conventional vision (it does not change the point of this paper) and from the calculated  $j_s^{2\text{D}}$  and  $j_s^{3\text{D}}$ , we extract  $\lambda_{\text{IEE}}$  that is found to be tunable from  $\lambda_{\text{IEE}} = 2 \text{ nm}$  near 0 V to a sharp maximum  $\lambda_{\text{IEE}} = 6 \text{ nm}$  at  $V_g = 200 \text{ V}$ , as shown in inset of Fig. 1(b) and in Ref. [9]. This very high value is comparable to that reported in the literature [7,8,11] and over one order of magnitude higher than that in the Ag/Bi interface  $\lambda_{\text{IEE}} = 0.3 \text{ nm}$  [5,6].

Now, we address the S/C conversion of our LAO/STO system in the THz frequency range. In this experiment, laser pulses at 800 nm (1.54 eV) with 150 fs duration are supplied by an amplified Ti-sapphire amplifier at a 1-kHz repetition rate. The absorption of the femtosecond pulse leads to the ultrafast demagnetization of the NiFe layer [26] triggering a burst of spin current injected into the 2DES and whose conversion into charge leads to the emission of the electromagnetic radiation at THz frequencies [29]. The signal is measured in the 300 GHz–3 THz range using electro-optic sampling in a 0.5-mm-thick (110) ZnTe crystal in air (see details of the experimental setup in [34]). The signals from NiFe/LAO/STO are directly compared with those from the CoFeB/Pt used

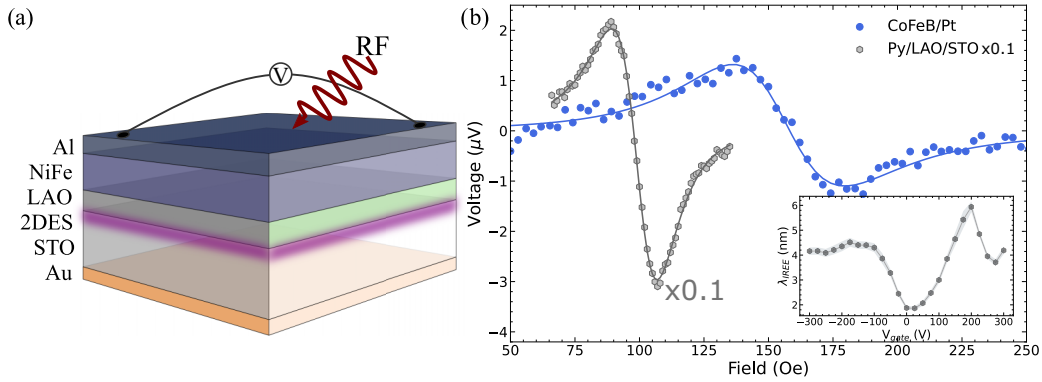


FIG. 1. (a) Spin pumping at 3.8 GHz for CoFeB(5)/Pt(3) in blue and at 3.2 GHz for SrTiO<sub>3</sub>/LaAlO<sub>3</sub>/NiFe(12) in grey (divided by 10), with their respective fits. The latter is at 10 K and with 200 V of back-gate voltage. After integration and fitting, the conversion efficiency of NiFe(12)/LaAlO<sub>3</sub>/SrTiO<sub>3</sub> is about ten times greater than that of CoFeB/Pt. The inset of (b) shows the back-gate voltage dependence of the effect (see Ref. [9]).

for comparison in the spin pumping experiment discussed above. In addition, THz emission from the LAO/STO sample was measured at variable temperature with an applied back-gate voltage. Note that all the THz responses have been measured for a pump fluence below 0.5 mJ/cm<sup>2</sup>, where their amplitude scales linearly with the incident density of optical energy.

Figure 2 shows the time-resolved magneto-optical curve along with the induced THz signals from the LAO/STO samples. The emission amplitudes in Fig. 2(c) are taken relative to that of a CoFeB(5 nm)/Pt(3 nm) sample. Therefore, the response in the picosecond range has lost about four orders of magnitude compared to the quasistatic one. This falls in the range of the emission from a pure ferromagnetic layer, as corroborated by a comparison with a sample where LaAlO<sub>3</sub> is grown on top of SrO terminated SrTiO<sub>3</sub> where the 2DES is not formed [37]. The absence of 2DES was also verified before depositing the NiFe injector, as the SrO-terminated sample is not conducting whereas the TiO<sub>2</sub>-terminated sample shows the characteristic room-temperature sheet resistance of a few kΩ [12]. Nevertheless, the measured THz emission from SrO and TiO<sub>2</sub> systems are roughly equivalent in amplitude, as shown in Fig. 2(b). This indicates that the ultrafast S/C conversion is likely to come from the ferromagnetic NiFe (including its interfaces with Al and LAO). From Fig. 2(b), one can note that the exact emission shape is different between the two samples which suggests that the 2DES contribution is probably opposite to that of the LAO/NiFe/Al and of a similar order of magnitude. This is confirmed by the weak temperature dependence visible in Fig. 2(c) where room temperature (black line) and 10 K with 200 V back-gate voltage applied (grey line) signals are rather similar. This is also consistent with the absence of back-gate dependence shown in Fig. 3(a), contrary to what is observed in the quasistatic range [Fig. 1(b)]. In addition, the spectral contents are also very similar [Fig. 3(b)]. One can possibly notice a slight shift towards higher frequencies for the SrO-terminated sample, suggesting that the 2DES emission contribution spectra is skewed towards lower frequencies.

Such a huge difference in efficiency between ISHE and IEE emitters at subpicosecond timescales has to stem from the conversion mechanism itself. The ISHE relies on

extrinsic, impurity scattering, and intrinsic mechanisms linked to the orbital momentum of the bands themselves [2,3,38]. The extrinsic contributions stem from spin-orbit coupling during scattering events leading to asymmetric skew and side-jump scattering from impurities. As electronic velocities in heavy metals (like Pt) only depend marginally on the electron energy for states close and well above the Fermi level, the ISHE mechanism is robust for high- and low-energy spin carriers. Therefore, the mechanism is as efficient for spin pumping, where spin excitations take place very close to the Fermi level, as for ultrafast demagnetization phenomena, where the electronic energy distribution can be rather broad, band structure dependent, and even structured [24,39]. It was actually reported to spread up to about 1.5 eV from the Fermi level in the early stage of the optical excitation, with a typical center weight of around 0.2 eV for thermalized carriers at relevant timescales [39]. This is potentially a huge drawback for IEE systems for which the effective Rashba split bands occupy well-defined energy levels. Because of this spread in energy, several bands can potentially simultaneously participate with different signs for the S/C conversion. Their existence has been demonstrated in LaAlO<sub>3</sub>/SrTiO<sub>3</sub>, where the back-gate voltage allows one to scan the different bands involved in the conversion [7]. Another important parameter has to be considered here as the LaAlO<sub>3</sub>/SrTiO<sub>3</sub> 2DES has a spin relaxation time two orders of magnitude larger than that in metals. This property, which has been coined to explain the efficiency of the dc S/C conversion effect [8], could be a disadvantage for an efficient THz response. We will try here to scrutinize in some detail the quantitative effects of these different mechanisms.

We build here a toy model to estimate the effect of two key timescales associated to the energy relaxation of the carriers carrying angular momentum and the spin lifetime in the 2DES. We start by considering that the process of demagnetization and remagnetization creates a short-lived non-equilibrium magnetization  $M(t)$  during which some angular momentum is transferred to the underlying electrons existing in the 2DES at the LAO/STO interface. The transfer mechanism is likely to rely on tunneling of the unbalanced spin population through the LAO barrier [40]. The complete process of “tunneling spin galvanic effect” is rather complex

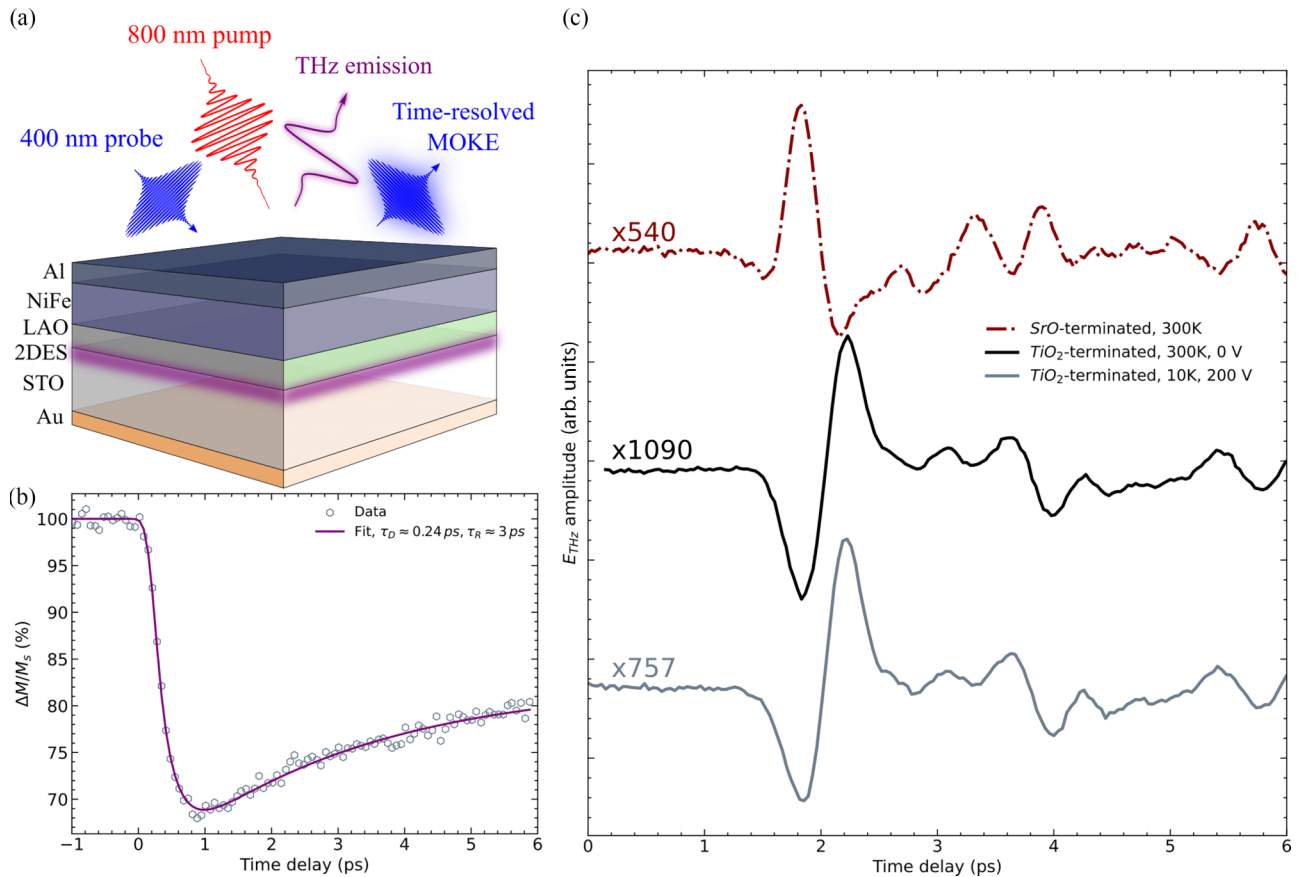


FIG. 2. Ultrafast measurements. (a) Setup schematics where an 800-nm pump pulse impinges on the top of the bilayer and the THz radiation is collected from the same side, in a specular geometry. A 400-nm probe is also used in reflection for magneto-optical Kerr effect (MOKE) measurements. (b) Time-resolved MOKE showing the demagnetization/remagnetization process of the NiFe along with the fits using two decreasing exponential functions. (c) The THz wave form recorded for the NiFe(12 nm)/LaAlO<sub>3</sub>(5 u.c.)/SrTiO<sub>3</sub> sample is measured at a temperature of 300 K (black) and at 10 K under 200-V back-gate voltage (grey). The raw signals are multiplied by the value indicated on the curves for a quantitative comparison to that of the CoFeB(5 nm)/Pt(3 nm) emitter at room-temperature (taken equal to 1). This is also compared to an equivalent sample (dotted, red) where the 2DES is absent (LAO is grown on top of a SrO-terminated SrTiO<sub>3</sub>).

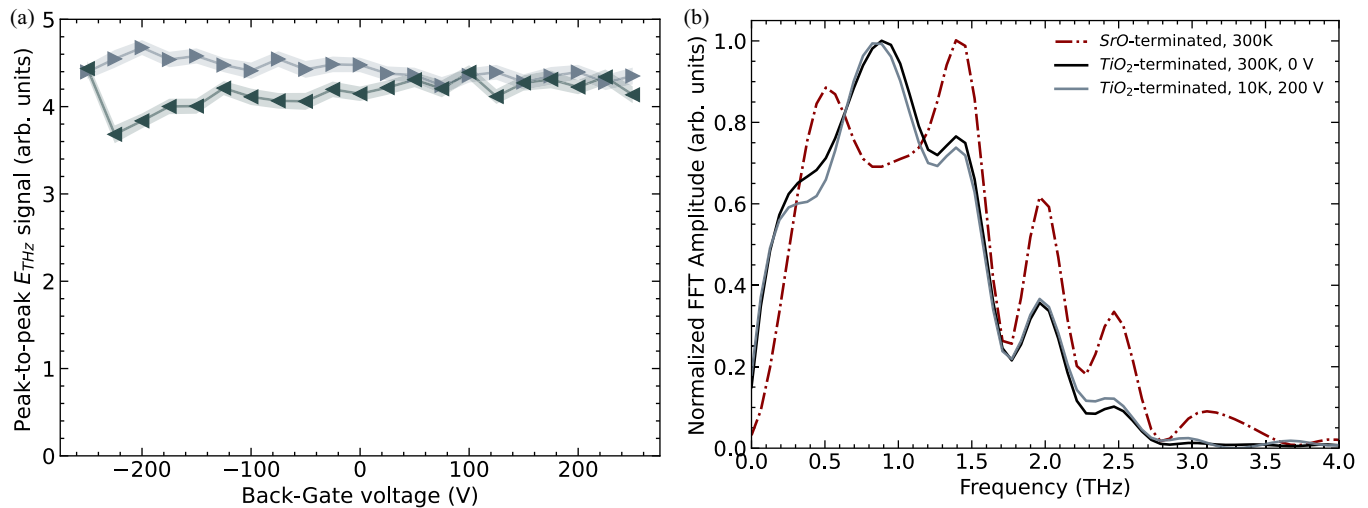


FIG. 3. (a) Back-gate dependence of the emitted THz signals: the values are differences between the two extrema of the bipolar responses from individual THz emission curves as in Fig. 2(c), measured for every back-gate voltage. No back-gate dependence is detected, in sharp contrast with the dc measurements (Fig. 1), showing a significant variation with a maximum at 200V. (b) Fast Fourier transform showing a global similar spectral content for all LAO/STO systems (the oscillations are due to absorption from the water in air).

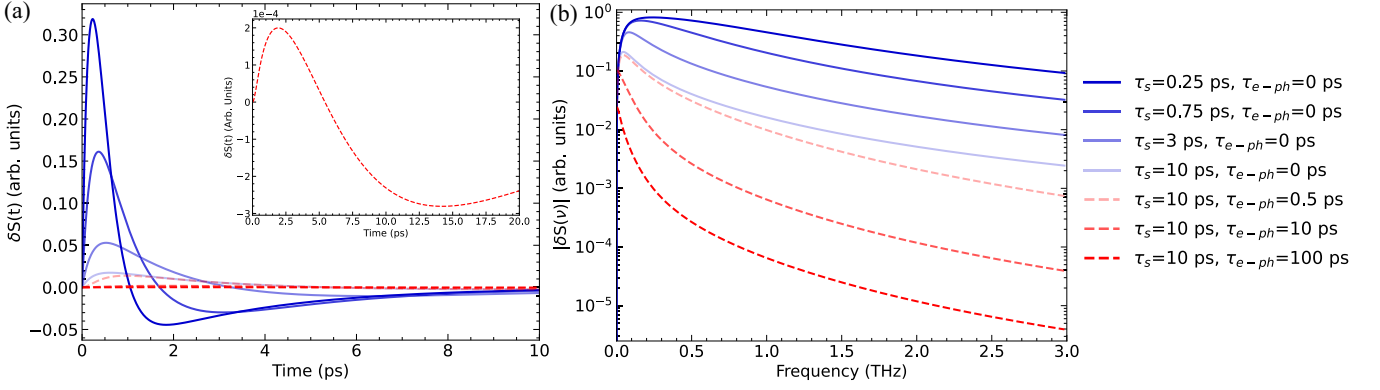


FIG. 4. Left panel: Time profile of the spin galvanic current  $J(t)$  for different values of the 2DES spin relaxation time:  $\tau_s/\tau_1 = 1, 3, 12$ , and 40 taking  $\tau_1 = 0.25$  ps,  $\tau_2 = 12\tau_1 = 3$  ps, and  $\tau_{e-ph}/\tau_1 = 0$  (blue curves), as well as curves with different values of the 2DES inelastic relaxation time:  $\tau_{e-ph} = 0, 5, 10, 100$  ps, taken for  $\tau_1 = 0.25$  ps,  $\tau_2 = 12\tau_1 = 3$  ps,  $\tau_s = 40$  ps,  $\tau_1 = 10$  ps (red dashed lines). Right panel: Fourier transform of the time profiles. It is seen that a long 2DES spin relaxation time of 10 ps shifts the main Fourier component to lower frequencies thus diminishing the S/C conversion at 1 THz by a factor 70. Another two orders of magnitude are lost by considering the inefficiency of the conversion for hot electrons, before their relaxation via inelastic scattering.

and a microscopic theory in the steady state is presented in Ref. [41]. Not entering into details, we admit here that a nonequilibrium spin polarization  $\delta S_0$  is created in the 2DES on the scale of the very short spin relaxation time in NiFe during laser-induced ultrafast demagnetization [Fig. 2(b)]. It is common practice to fit this behavior using two decreasing exponentials with characteristic times  $\tau_1$  and  $\tau_2$ , accounting for the demagnetization and the remagnetization processes in the form

$$M(t) = M_0[1 - \theta(t)(e^{-t/\tau_1} - e^{-t/\tau_2})], \quad (1)$$

with  $\theta(t)$  the step function. At every instant the spin transferred per unit time to the LAO/STO 2DEG is proportional to the time derivative of  $M$ :

$$\Gamma(t) = A dM(t)/dt = AM_0\theta(t)[e^{-t/\tau_1}/\tau_1 - e^{-t/\tau_2}/\tau_2] \quad (2)$$

with  $A$  a constant accounting for all complex transfer mechanisms through the tunnel barrier. This spin injection rate is counterbalanced by the dissipation of angular momentum through a typical spin relaxation time  $\tau_s$  leading to the rate equation for the nonequilibrium spin accumulation in the 2DEG:

$$\partial_t \delta S = -\frac{\delta S}{\tau_s} + \Gamma(t). \quad (3)$$

$\tau_s$  can have different origins including Elliott-Yafet ( $\tau_{EY}$ ) and Dyakonov-Perel ( $\tau_{DP}$ ) mechanisms, as well as the escape time of the 2DES electrons through the LAO tunnel barrier ( $\tau_\lambda$ ). In LAO/STO, the latter is the shortest because the 2DES is a very clean system ( $\tau_{DP,EY} > \tau_\lambda$ ) [12,17]. Thus, one has  $\tau_s \sim \tau_\lambda$  which is usually much greater than  $\tau_1$  and of a similar order of magnitude as the remagnetization time  $\tau_2$ . This influences the spin accumulation stemming from the spin pulse (demagnetization and then remagnetization), whose expression can be obtained by a sequence of

Fourier-transforms:

$$\Gamma(\omega) = AM_0 \left\{ \frac{1}{(i\omega\tau_1 - 1)} - \frac{1}{(i\omega\tau_2 - 1)} \right\}, \quad (4)$$

$$\begin{aligned} \delta S(\omega) &= -\frac{\tau_s}{1 - i\omega\tau_s} \Gamma(\omega) \\ &= AM_0 \left\{ \frac{-1}{\left(\frac{i\tau_1}{\tau_s} + \tau_1\omega\right)(i\omega\tau_1 - 1)} \right. \\ &\quad \left. + \frac{1}{\left(\frac{i\tau_2}{\tau_s} + \tau_2\omega\right)(i\omega\tau_2 - 1)} \right\}, \quad (5) \end{aligned}$$

and

$$\delta S(t) = AM_0\tau_s \left\{ \left[ \frac{e^{-t/\tau_1} - e^{-t/\tau_s}}{\tau_1 - \tau_s} \right] - \left[ \frac{e^{-t/\tau_2} - e^{-t/\tau_s}}{\tau_2 - \tau_s} \right] \right\} \theta(t). \quad (6)$$

This is therefore the time dependence of the spin polarized population inside the 2DES. Its profile  $\delta S(t)$  is shown in Fig. 4(a) for the following values of the relevant parameters:  $AM_0 = 1$ ,  $\tau_1 = 0.25$  ps,  $\tau_2 = 3$  ps =  $12\tau_1$ ,  $\tau_s = 10$  ps =  $40\tau_1$ , and for different ratios between spin relaxation and demagnetization times. It can be seen in Fig. 4 that accounting for the different timescales already decreases the amplitude of the response by a factor 50 while also shifting it to lower frequencies. Indeed as  $\tau_s$  increases, the spin accumulation progressively departs from a  $dM(t)/dt$  behavior and tends towards a  $M(t)$  dependence as can be seen directly in the rate evolution Eq. (3). This slows down the process, resulting in a different frequency fingerprint and a 50-fold loss of amplitude at 1 THz. Although this is already significant, it cannot fully explain the four orders of magnitude loss observed in the measurements and another physical effect must be at play.

We suggest here that because this nonequilibrium spin polarization  $\delta S(t)$  is due to hot-electron injection from the FM, it cannot be straightforwardly converted into a charge

current via the spin galvanic effect, since such electrons are away from the Rashba-effective energy region of the 2DEG. We postulate here that the spread in energy leads to a very inefficient conversion until the angular momentum carrying entities relax in energy close to the Fermi level. This is very slow in the LAO/STO system [42] because the  $t_{2g}$  splitting imposes several interband transitions before reaching the final state. Furthermore, hot carriers form polarons in highly polar STO which drastically reduces relaxation times [43]. This phenomenon is absent in metallic structures like NiFe/Bi/Ag or CoFeB/MgO due to the small polarizability of the lattice. As a result, apart from a small intraband contribution in the 2DES [42] (giving a Drude contribution below 5 ps), the carrier relaxation time exceeds 100 ps. As this is larger than the escape time through the tunnel barrier, the majority of electrons in the 2D gas are very likely spread in energies within  $\sim 1$  eV above the Fermi level. This is of course problematic for the conversion into charge as hot carriers also have to relax in energy without losing their angular momentum in the process. In order to assess the induced efficiency loss, we assume that the “useful” nonequilibrium spin polarization from low-energy electrons is

$$\delta\bar{S}(t) = [1 - e^{-t/\tau_{e-ph}}]\delta S(t)$$

with  $\tau_{e-ph}$  the effective inelastic electron-phonon relaxation time taking into account all aforementioned slow processes. The expected spin galvanic current will then be  $I(t) \sim \alpha_R \delta\bar{S}(t)$ , with  $\alpha_R$  the effective Rashba constant. Figure 4 plots the ratio between this current (normalized by that for CoFeB/Pt) and the expected dc conversion (also normalized by that for CoFeB/Pt in the dc regime) for different values of  $\tau_{e-ph}$  (note that this normalization with our “standard” CoFeB/Pt introduces an extra division by  $\tau_s$ ).

This has two effects. The first one is a dramatic decrease of signal amplitude as the angular momentum is lost while electrons are still not thermalized (and form self-trapped polarons), thus leading to a huge waste of conversion efficiency. Moreover, because hot electrons are known to enhance inelastic tunneling through oxygen vacancies in STO [44], it is very likely that this process decreases the escape time and does not conserve the angular momentum of the charge carriers, reinforcing again the inefficiency of hot electron transport. The second effect is a shift of the spectral content of the conversion current to lower frequencies, thus escaping further the THz band and the lower limit of our detection. Figure 4 shows that it is easy to lose three orders of magnitude taking reasonable parameters for the LAO/STO system. We point out here that the exact line shape of the 2DES contribution should

indeed be smoother than that measured [see Fig. 4(a)] but it is filtered out by our detection and hidden by the dominant signal directly from the ferromagnetic layer.

In conclusion, we have experimentally demonstrated the drastic decrease in the efficiency of the IEE spin-to-charge conversion mechanism between quasi-DC and subpicosecond timescales in the LAO/STO system. This effect is explained by the energy-dependent splitting of the Rashba bands [32] associated with the slow thermalization of the injected hot angular momentum carriers. The long spin lifetime in the 2DES also participates in the inefficiency of the LAO/STO system for THz emission. To optimize THz emission, one should therefore seek large Rashba coefficients and low relaxation rates, i.e., largely split interface states in metals, like Bi/Ag vs LAO/STO. More generally, while THz emission can be reliably inferred from the dc behavior of ISHE materials for which spin dependent scattering is similar for hot and cold carriers, band structure calculations complemented by the time-resolved hot carrier distribution and relaxation are necessary to quantify the particular behavior of IEE systems. Moreover, we underline here that there is no conceptual difference between spin and orbital angular momentum conversion, so that the phenomenology developed here should be applicable to all IEE systems (even if orbital to charge conversion dominates as in LAO/STO [9]). We also suggest that the efficiency of THz emission could be optimized by adapting the Rashba splitting to the energy distribution of charge and spin carriers at the subpicosecond timescales.

We would like to acknowledge fruitful discussions with Jean-Marc Triscone (University of Geneva). We acknowledge funding from the French National Research Agency (ANR) through the SANTA (Grant No. ANR-18-CE24-0018-01), SPINUP (Grant No. ANR-21-CE24-0026-01), and ORION (Grant No. ANR-20-CE30-0022-03) projects, as well as SPICY from the Labex NanoSaclay Investissements d’Avenir program (Grant No. ANR-10-LABX-0035). This work was also supported by a government grant managed by the ANR as a part of the France 2030 investment plan from PEPR SPIN ANR-22-EXSP 0003 (moonshots TOAST and SPIN-CHARAC). This work was also supported by EIC Pathfinder OPEN Grant No. 101129641 “OBELIX.” Finally, the authors acknowledge the support team of the “Plateforme Laser femtoseconde” at IMMM, Le Mans University, where the THz experiments were conducted. A.L., V.J., G.V., and P.R. thank the Region Pays de la Loire, the FEDER, for funding support. C.G. acknowledges useful discussions with the STherQO members.

- 
- [1] S. A. Wolf, D. D. Awschalom, R. A. Buhrman, J. M. Daughton, M. L. Roukes, A. Y. Chtchelkanova, and D. M. Treger, Spintronics: A spin-based electronics vision for the future, *Science* **294**, 1488 (2001).
- [2] J. E. Hirsch, Spin Hall effect, *Phys. Rev. Lett.* **83**, 1834 (1999).
- [3] J. Sinova, D. Culcer, Q. Niu, N. A. Sinitsyn, T. Jungwirth, and A. H. MacDonald, Universal intrinsic spin Hall effect, *Phys. Rev. Lett.* **92**, 126603 (2004).

- [4] V. M. Edelstein, Spin polarization of conduction electrons induced by electric current in two-dimensional asymmetric electron systems, *Solid State Commun.* **73**, 233 (1990).
- [5] J.-C. Rojas-Sánchez, L. Vila, G. Desfonds, S. Gambarelli, J. P. Attané, J. M. D. Teresa, C. Magén, and A. Fert, Spin-to-charge conversion using Rashba coupling at the interface between non-magnetic materials, *Nat. Commun.* **4**, 2944 (2013).
- [6] S. Sangiao, J. M. De Teresa, L. Morellon, I. Lucas, M. C. Martinez-Velarte, and M. Viret, Control of the spin to charge

- conversion using the inverse Rashba-Edelstein effect, *Appl. Phys. Lett.* **106**, 172403 (2015).
- [7] E. Lesne, Y. Fu, S. Oyarzun, J. C. Rojas-Sánchez, D. C. Vaz, H. Naganuma, G. Sicoli, J.-P. Attané, M. Jamet, E. Jacquet *et al.*, Highly efficient and tunable spin-to-charge conversion through Rashba coupling at oxide interfaces, *Nat. Mater.* **15**, 1261 (2016).
- [8] J.-Y. Chauleau, M. Boselli, S. Gariglio, R. Weil, G. de Loubens, J.-M. Triscone, and M. Viret, Efficient spin-to-charge conversion in the 2D electron liquid at the LAO/STO interface, *Europhys. Lett.* **116**, 17006 (2016).
- [9] A. El Hamdi, J.-Y. Chauleau, M. Boselli, C. Thibault, C. Gorini, A. Smogunov, C. Barreateau, S. Gariglio, J.-M. Triscone, and M. Viret, Observation of the orbital inverse Rashba-Edelstein effect, *Nat. Phys.* **19**, 1855 (2023).
- [10] S. D. Ganichev, E. L. Ivchenko, V. V. Bel'kov, S. A. Tarasenko, M. Sollinger, D. Weiss, W. Wegscheider, and W. Prettl, Spin-galvanic effect, *Nature (London)* **417**, 153 (2002).
- [11] D. C. Vaz *et al.*, Mapping spin-charge conversion to the band structure in a topological oxide two-dimensional electron gas, *Nat. Mater.* **18**, 1187 (2019).
- [12] A. D. Caviglia, M. Gabay, S. Gariglio, N. Reyren, C. Cancellieri, and J.-M. Triscone, Tunable Rashba spin-orbit interaction at oxide interfaces, *Phys. Rev. Lett.* **104**, 126803 (2010).
- [13] A. D. Caviglia, S. Gariglio, N. Reyren, D. Jaccard, T. Schneider, M. Gabay, S. Thiel, G. Hammerl, J. Mannhart, and J.-M. Triscone, Electric field control of the LaAlO<sub>3</sub>/SrTiO<sub>3</sub> interface ground state, *Nature (London)* **456**, 7222 (2008).
- [14] A. Joshua, S. Pecker, J. Ruhman, E. Altman, and S. Ilani, A universal critical density underlying the physics of electrons at the LaAlO<sub>3</sub>/SrTiO<sub>3</sub> interface, *Nat. Commun.* **3**, 1129 (2012).
- [15] A. Joshua, J. Ruhman, S. Pecker, E. Altman, and S. Ilani, Gate-tunable polarized phase of two-dimensional electrons at the LaAlO<sub>3</sub>/SrTiO<sub>3</sub> interface, *Proc. Natl. Acad. Sci. USA* **110**, 9633 (2013).
- [16] K. V. Shanavas, Z. S. Popović, and S. Satpathy, Theoretical model for Rashba spin-orbit interaction in d electrons, *Phys. Rev. B* **90**, 165108 (2014).
- [17] M.-J. Jin *et al.*, Nonlocal spin diffusion driven by giant spin Hall effect at oxide heterointerfaces, *Nano Lett.* **17**, 36 (2017).
- [18] F. Trier *et al.*, Electric-field control of spin current generation and detection in ferromagnet-free SrTiO<sub>3</sub>-based nanodevices, *Nano Lett.* **20**, 395 (2020).
- [19] J. Sinova, S. O. Valenzuela, J. Wunderlich, C. H. Back, and T. Jungwirth, Spin Hall effects, *Rev. Mod. Phys.* **87**, 1213 (2015).
- [20] E. Beaurepaire, J.-C. Merle, A. Daunois, and J.-Y. Bigot, Ultrafast spin dynamics in ferromagnetic nickel, *Phys. Rev. Lett.* **76**, 4250 (1996).
- [21] J.-Y. Bigot and M. Vomir, Ultrafast magnetization dynamics of nanostructures: Ultrafast magnetization dynamics of nanostructures, *Ann. Phys.* **525**, 2 (2013).
- [22] J. Walowski and M. Münzenberg, Perspective: Ultrafast magnetism and THz spintronics, *J. Appl. Phys.* **120**, 140901 (2016).
- [23] M. Battiato, K. Carva, and P. M. Oppeneer, Superdiffusive spin transport as a mechanism of ultrafast demagnetization, *Phys. Rev. Lett.* **105**, 027203 (2010).
- [24] A. Melnikov, I. Rzdolski, T. O. Wehling, E. Th. Papaioannou, V. Roddatis, P. Fumagalli, O. Aktsipetrov, A. I. Lichtenstein, and U. Bovensiepen, Ultrafast transport of laser-excited spin-polarized carriers in Au/Fe/MgO (001), *Phys. Rev. Lett.* **107**, 076601 (2011).
- [25] A. Alekhin *et al.*, Femtosecond spin current pulses generated by the nonthermal spin-dependent Seebeck effect and interacting with ferromagnets in spin valves, *Phys. Rev. Lett.* **119**, 017202 (2017).
- [26] T. Kampfrath *et al.*, Terahertz spin current pulses controlled by magnetic heterostructures, *Nat. Nanotechnol.* **8**, 256 (2013).
- [27] E. Beaurepaire, G. M. Turner, S. M. Harrel, M. C. Beard, J.-Y. Bigot, and C. A. Schmuttenmaer, Coherent terahertz emission from ferromagnetic films excited by femtosecond laser pulses, *Appl. Phys. Lett.* **84**, 3465 (2004).
- [28] D. J. Hilton, R. D. Averitt, C. A. Meserole, G. L. Fisher, D. J. Funk, J. D. Thompson, and A. J. Taylor, Terahertz emission via ultrashort-pulse excitation of magnetic metal films, *Opt. Lett.* **29**, 1805 (2004).
- [29] T. Seifert *et al.*, Efficient metallic spintronic emitters of ultrabroadband terahertz radiation, *Nat. Photonics* **10**, 483 (2016).
- [30] A. Rice, Y. Jin, X. F. Ma, X.-C. Zhang, D. Bliss, J. Larkin, and M. Alexander, Terahertz optical rectification from (110) zinc-blende crystals, *Appl. Phys. Lett.* **64**, 1324 (1994).
- [31] M. B. Johnston, D. M. Whittaker, A. Corchia, A. G. Davies, and E. H. Linfield, Simulation of terahertz generation at semiconductor surfaces, *Phys. Rev. B* **65**, 165301 (2002).
- [32] C. Zhou, Y. P. Liu, Z. Wang, S. J. Ma, M. W. Jia, R. Q. Wu, L. Zhou, W. Zhang, M. K. Liu, Y. Z. Wu, and J. Qi, Broadband terahertz generation via the interface inverse Rashba-Edelstein effect, *Phys. Rev. Lett.* **121**, 086801 (2018).
- [33] M. B. Jungfleisch, Q. Zhang, W. Zhang, J. E. Pearson, R. D. Schaller, H. Wen, and A. Hoffmann, Control of terahertz emission by ultrafast spin-charge current conversion at Rashba interfaces, *Phys. Rev. Lett.* **120**, 207207 (2018).
- [34] A. Levchuk, V. Juvé, T. O. Otomalo, T. Chirac, O. Rousseau, A. Solognac, G. Vaudel, P. Ruello, J.-Y. Chauleau, and M. Viret, Pump wavelength-dependent terahertz spin-to-charge conversion in CoFeB/MgO Rashba interface, *Appl. Phys. Lett.* **123**, 012407 (2023).
- [35] G. Wei, Z. Hui, X. Wu, H. Zhang, W. Chun, B. Wang, W. Li, and S. Jirong, Terahertz emission from LAO/STO heterostructures with femtosecond laser pumping, *Acta Phys. Sin.* **71**, 090702 (2022).
- [36] Y. Tserkovnyak, A. Brataas, and G. E. W. Bauer, Spin pumping and magnetization dynamics in metallic multilayers, *Phys. Rev. B* **66**, 224403 (2002).
- [37] J. Nishimura, A. Ohtomo, A. Ohkubo, Y. Murakami, and M. Kawasaki, Controlled carrier generation at a polarity-discontinued perovskite heterointerface, *Jpn. J. Appl. Phys.* **43**, L1032 (2004).
- [38] S. Murakami, Dissipationless quantum spin current at room temperature, *Science* **301**, 1348 (2003).
- [39] H.-S. Rhie, H. A. Dürr, and W. Eberhardt, Femtosecond electron and spin dynamics in Ni/W(110) films, *Phys. Rev. Lett.* **90**, 247201 (2003).
- [40] N. Reyren, M. Bibes, E. Lesne, J.-M. George, C. Deranlot, S. Collin, A. Barthélémy, and H. Jaffrès, Gate-controlled spin injection at LaAlO<sub>3</sub>/SrTiO<sub>3</sub> interfaces, *Phys. Rev. Lett.* **108**, 186802 (2012).

- [41] G. Fleury, M. Barth, and C. Gorini, Tunneling anisotropic spin galvanic effect, *Phys. Rev. B* **108**, L081402 (2023).
- [42] Y. Yamada, H. K. Sato, Y. Hikita, H. Y. Hwang, and Y. Kanemitsu, Measurement of the femtosecond optical absorption of LaAlO<sub>3</sub>/SrTiO<sub>3</sub> heterostructures: Evidence for an extremely slow electron relaxation at the interface, *Phys. Rev. Lett.* **111**, 047403 (2013).
- [43] J. T. Devreese, S. N. Klimin, J. L. M. van Mechelen, and D. van der Marel, Many-body large polaron optical conductivity in SrTi<sub>1-x</sub>Nb<sub>x</sub>O<sub>3</sub>, *Phys. Rev. B* **81**, 125119 (2010).
- [44] J. Jeon, K. Eom, Y. Hong, C.-B. Eom, K. Heo, and H. Lee, Hot electron tunneling in Pt/LaAlO<sub>3</sub>/SrTiO<sub>3</sub> heterostructures for enhanced photodetection, *ACS Appl. Mater. Interfaces* **13**, 47208 (2021).